ACS OMEGA

http://pubs.acs.org/journal/acsodf

Article

Chemometric Classification of Oil Families in the Laizhouwan Depression, Bohai Bay Basin, Eastern China

Zhongjian Tan, Jiawei Guo, and Haiping Huang*

Cite This: *ACS Omega* 2021, 6, 24106−24117

Read Online

ACCESS | Metrics & More | Article Recommendations

ABSTRACT: A suite of oil-sand bitumen and crude oil samples, collected from the Laizhouwan depression, Bohai Bay basin, were geochemically investigated for molecular compositions. Three oil families (A, B, and C) were classified by hierarchical cluster analysis (HCA) and principal component analysis on nine typical biomarker ratios. Typically, family A oils are characterized by relatively low values of gammacerane/C_{31} homohopane 22R (G/H31, 0.13−0.76) and C_{35}/C_{34} homohopane (H35/H34, 0.39−0.78), suggesting a source from freshwater depositional environments. In contrast, family C oils show a relatively high G/H31 (2.49−5.41) and H35/H34 (1.43−2.45) ratios, indicating a source from hypersaline water depositional environments. Family B oils display ratios of G/H31 and H35/H34 in-between the range of families A and C, suggesting mixed origin. In addition, family A oils can be further classified into four subfamilies (A1, A2, A3, and A4) and family B oils into two subfamilies (B1 and B2) by HCA. The A1 oils characterized by a high C_{24} tetracyclic terpane/C_{26} tricyclic terpane (TeT24/TT26) ratio (1.02−1.39) are mainly distributed in the northeast, B1 oils characterized by relatively low TeT24/TT26 ratio are in the west, and A2, A3, and A4 oils with an intermediate TeT24/TT26 ratio are in the center of the depression. Oils in well L16-1-2 in the southern depression, however, show vertical variations with family C oils in the deeper reservoirs, subfamily B2 oils in the shallower reservoirs, and subfamily A4 oils in the middle-depth reservoirs. Based on the biomarker compositions, at least three oil charges were indicated: family C oils are likely sourced from the Es4 rock in the southern sag, B2 oils may be a mixture of family C with family A oils, and A4 oils without biodegradation influence may be the latest charge derived from the Es3 source rock in the northern sag. The oil families and/or subfamilies with typical genetic affinities, as well as the regular occurrence in different blocks, may indicate two major petroleum systems or multiple subsidiary oil systems existing in the Laizhouwan depression.

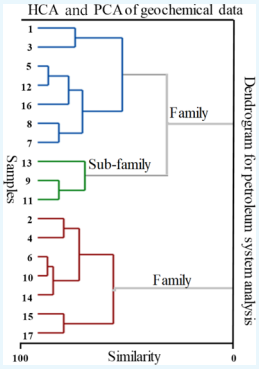

1. INTRODUCTION

The Laizhouwan depression is located in the southern part of the offshore Bohai Bay basin. With over a decade of petroleum exploration, plenty of petroleum resources have been discovered despite its limited size, showing prospective petroleum potentials.[1−5] The Kenli10-1 oilfield, located at the northern steep slope zone, was the first petroleum discovery with 10^8 ton reserves in 2008. Afterward, a series of oilfields were revealed to be distributed almost all over the depression. Limited geochemical studies on the source and sedimentary features in the Laizhouwan depression have been reported in the literature. Good source rocks were developed within the third member (Es3) and the fourth member (Es4) of the Shahejie formation.[1] Typical biomarkers revealed in the oils from the Kenli10-1 oilfield indicate a source from freshwater depositional environments.[3,5] More recently, a set of high-sulfuric oils were observed in the southern part of the depression, suggesting a source from saline water depositional environments likely developed in the Es4 member within the southern sag.[6] Typical biomarker compositions in the oils have been successfully applied to oil-source correlation and validated two end-member systems in the depression.[7,8] Generally, crude oils were revealed to be widespread in the depression with reservoirs vertically distributed in the Minghuazhen (Nm), Guantao (Ng), Dongying (Ed), Shahejie (Es), and Kongdian (Ek) formations. The oils produced from different formations show great variability in physical properties with API (American Petroleum Institute) gravity ranging in 14−35° and viscosity changing in 6.5−2283 mPa·s. However, detailed oil classification and regional occurrence have not been documented yet. Oil family classification is closely related to the potential source rock distribution and petroleum system identification, which governs the resource assessment and exploration potential verification. In this study, we use the chemometric method to identify the oil families and/or subfamilies in the study area on the basis of molecular compositions, which have not been altered by biodegradation. The aim of the present study is to have a well understanding

Received: July 8, 2021
Published: September 8, 2021

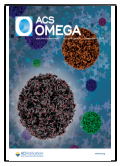

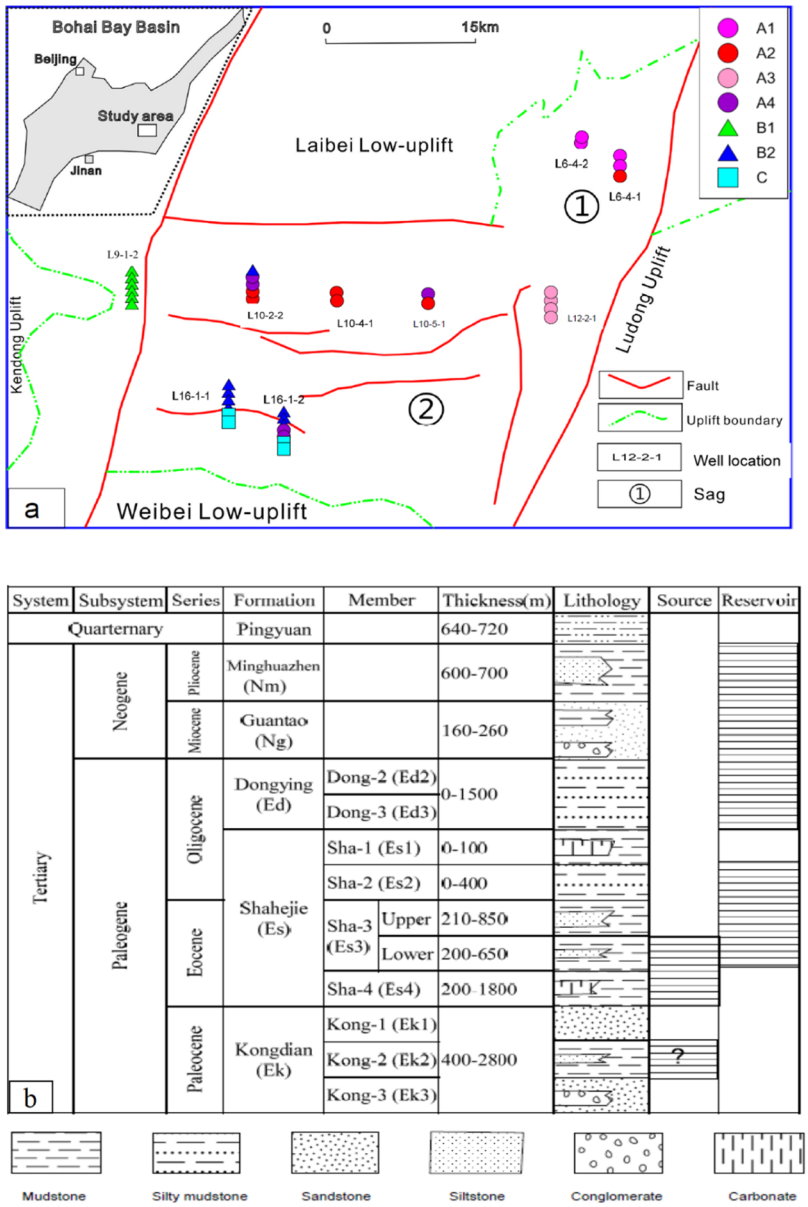

Figure 1. (a) Sketch map showing the location and geological setting of the Laizhouwan depression with occurrence of oil groups/subgroups; (b) generalized stratigraphy of the Laizhouwan depression, possible source rock, and major reservoir intervals marked.

the occurrence of petroleum systems and to facilitate further exploration and resource assessment within the Laizhouwan depression.

2. GEOLOGICAL SETTING

The Bohai Bay basin, one of the most petroliferous basins in China, is situated on the eastern coast of China (Figure 1a). Basic petroleum geology in terms of structural unit division, sedimentary history, lithology of the Cenozoic strata, and oil and gas distribution has been well documented by numerous studies.[9−12] A complex evolution history during the tertiary period resulted in a series of grabens and half-grabens developed into subbasins, each of which has its independent petroleum systems.

The Laizhouwan depression, one of the secondary structural units located in southern Bohai Bay basin, covers an area about 1780 km^2 and is bordered by the Kendong Uplift to the west, the Ludong Uplift to the east, the Weibei Low-Uplift to the south, and the Laibei Low-Uplift to the north with northeastern sag ① and main sag ② as two main depocenters (Figure 1a).[8,13,14] The strata developed in the depression include the Paleogene (Kongdian, Shahejie, and Dongying formations), the Neogene (Guantao and Minghuazhen formations), and the Quaternary Pingyuan Formation (Figure 1b). The evolution of the Laizhouwan depression in the Cenozoic era can be divided into four stages: rifting stage (from the Kongdian period to Es3 period), rifting-depression stage (from the Es2 period to Ed period), postrift depression stage (from Ed1 period to Ng period), and neotectonism-related postrift depression stage (from Nm period to now).[16]

The Kongdian Formation, unconformably overlaid on the Mesozoic strata, principally comprises mudstone, black shale, sandstone, siltstone, basalt, and conglomerate with limited hydrocarbon generation potential. The Shahejie Formation can be divided into four members: Es1, Es2, Es3, and Es4, from the top to the base. The Es4 member was deposited in a

https://doi.org/10.1021/acsomega.1c03598
ACS Omega 2021, 6, 24106−24117

Table 1. Basic Geological Information and Geochemical Parameters for Samples from the Laizhouwan Depression

											parameters used for HCA and PCA								
well	depth/m	Fm	sample	family	subfamily	PM level[a]	Pr/Ph	Pr/C_{17}	Ph/C_{18}	31S/R	29S/R	29β/α	T20/23	Te24/T26	ETR	Ts/Tm	29Ts/H	G/H31	H35/34
L6-4-1	2153−2182	Ed	oil	A	A1	0	0.94	0.57	0.6	0.58	0.29	0.31	0.48	1.39	0.18	0.68	0.34	0.36	0.57
L6-4-1	2455	Ed	oil sand	A	A1	0	0.97	0.57	0.51	0.58	0.28	0.3	0.44	1.24	0.12	0.7	0.36	0.31	0.53
L6-4-2	2561−2565	Es2	oil	A	A1	0	0.57	0.66	0.74	0.58	0.3	0.3	0.38	1.26	0.22	0.55	0.27	0.29	0.57
L6-4-2	2585−2603	Es2	oil	A	A1	0	0.6	0.71	0.76	0.57	0.3	0.3	0.35	1.02	0.23	0.56	0.27	0.31	0.65
L6-4-1	3457−3484	Es3	oil	A	A2	0	1.05	0.32	0.29	0.59	0.4	0.44	0.51	1.25	0.18	1.17	0.46	0.28	0.52
L10-2-2	2624	Es3	oil sand	A	A2	0	0.32	0.36	0.51	0.59	0.34	0.38	0.31	0.86	0.33	1.32	0.41	0.17	0.39
L10-2-2	2966.5	Es3	oil sand	A	A2	0	0.56	0.37	0.27	0.6	0.35	0.38	0.28	0.91	0.34	1.27	0.38	0.16	0.41
L10-4-1	2113−2122	Es3	oil	A	A2	0	0.91	0.5	0.52	0.58	0.44	0.43	0.38	0.9	0.34	1.02	0.35	0.17	0.53
L10-4-1	2174−2185	Es3	oil	A	A2	0	0.91	0.47	0.51	0.58	0.44	0.44	0.39	0.89	0.34	1.05	0.35	0.13	0.51
L10-5-1	1599.5	Ed	oil	A	A2	0	0.69	2.08	1.25	0.6	0.42	0.46	0.49	0.91	0.33	1.31	0.4	0.24	0.58
L12-2-1	566	Ed	oil sand	A	A3	2−3				0.58	0.35	0.44	0.75	0.78	0.25	1.52	0.51	0.56	0.42
L12-2-1	570−578	Ed	oil	A	A3	2−4				0.59	0.47	0.49	0.65	0.79	0.25	1.6	0.42	0.36	0.42
L12-2-1	598	Ed	oil sand	A	A3	2−3				0.57	0.4	0.45	0.7	0.73	0.27	1.36	0.5	0.36	0.42
L12-2-1	627−637	Ed	oil	A	A3	2−4				0.58	0.47	0.49	0.62	0.84	0.28	1.44	0.41	0.31	0.42
L10-2-2	1474	Nm	oil sand	A	A4	4−6				0.63	0.41	0.44	0.47	0.95	0.42	1.26	0.56	0.5	0.66
L10-2-2	1553	Ng	oil sand	A	A4	3−4				0.6	0.35	0.45	0.34	0.95	0.42	0.97	0.33	0.56	0.55
L10-5-1	1251	Nm	oil	A	A4	3−7				0.67	0.38	0.45	0.5	0.98	0.46	1.13	0.4	0.76	0.78
L16-1-2	1079	Es3	oil sand	A	A4	0	0.67	0.66	1.03	0.58	0.35	0.42	0.52	0.83	0.35	1.37	0.43	0.6	0.72
L16-1-2	1107	Es3	oil sand	A	A4	0	0.65	0.46	0.75	0.58	0.32	0.42	0.47	0.81	0.36	1.33	0.42	0.58	0.71
L9-1-2	892	Nm	oil sand	B	B1	3−5				0.57	0.37	0.44	0.45	0.75	0.31	1.61	0.55	0.75	0.51
L9-1-2	1137	Nm	oil sand	B	B1	3−5				0.57	0.37	0.42	0.4	0.61	0.4	1.6	0.87	1.37	0.54
L9-1-2	1158.9	Nm	oil sand	B	B1	3−5				0.57	0.37	0.43	0.43	0.66	0.37	1.71	0.78	1.16	0.54
L9-1-2	1204	Nm	oil sand	B	B1	3−5				0.58	0.38	0.44	0.55	0.69	0.34	1.86	0.86	0.98	0.53
L9-1-2	1271	Ng	oil sand	B	B1	3−5				0.57	0.38	0.46	0.42	0.6	0.34	2.03	0.82	0.92	0.58
L9-1-2	1306	Ng	oil sand	B	B1	3−5				0.57	0.39	0.45	0.42	0.62	0.32	1.98	0.78	0.96	0.72
L10-2-2	1399	Nm	oil sand	B	B2	4−6				0.63	0.4	0.44	0.45	0.94	0.41	1.22	0.47	1.48	0.72
L16-1-1	934	Nm	oil sand	B	B2	2−4	0.29	3.5	7.21	0.59	0.34	0.48	0.39	1	0.4	1.05	0.37	1.25	1.01
L16-1-1	937.5	Nm	oil	B	B2	2−4	0.36	3.12	6.85	0.59	0.33	0.47	0.46	0.93	0.41	1.03	0.37	1.3	1.18
L16-1-1	969	Ng	oil sand	B	B2	2−3	0.24	3.37	7.3	0.6	0.35	0.48	0.34	0.99	0.4	1.03	0.38	1.31	1
L16-1-1	980	Ng	oil sand	B	B2	2−3	0.23	2.17	5.04	0.6	0.34	0.47	0.35	1.01	0.4	1.04	0.38	1.31	1
L16-1-2	974.76	Ng	oil sand	B	B2	2−4	0.52	3.75	11.97	0.58	0.33	0.46	0.53	0.95	0.44	1.03	0.35	1.39	1.13
L16-1-2	978	Ng	oil sand	B	B2	2−4	0.54	2.56	9.88	0.59	0.32	0.46	0.49	0.93	0.42	1.02	0.35	1.38	1.15
L16-1-2	992	Ng	oil sand	B	B2	2−4	0.59	1.16	4.77	0.59	0.33	0.46	0.48	0.94	0.43	0.98	0.39	1.29	1.21
L16-1-1	1024	Ng	oil sand	C		2−4	0.21	1.4	3.01	0.59	0.39	0.55	0.33	1.17	0.47	0.6	0.28	2.49	1.43
L16-1-1	1141	Ek	oil sand	C		2−3	0.32	0.62	0.95	0.57	0.56	0.69	0.33	1.29	0.51	0.4	0.14	3.77	1.77
L16-1-2	1206.5	Es3	oil sand	C		2−3	0.21	3.69	14.4	0.55	0.28	0.36	0.46	1.41	0.56	0.28	0.14	5.41	2.45
L16-1-2	1281	Ek	oil sand	C		2−3	0.24	0.6	3.02	0.56	0.29	0.36	0.48	1.43	0.56	0.32	0.15	5.28	2.21

[a]PM level: level of biodegradation on Peters and Moldowan (1993) scale; Pr/Ph: pristane/phytane; Pr/C_{17}: pristane/*n*-C_{17}; Ph/C_{18}: phytane/*n*-C_{18}; 31S/R: C_{31} homohopane 22S/(22S + 22R); 29S/R: C_{29} $\alpha\alpha\alpha$ sterane 20S/(20S + 20R); 29β/α: C_{29} sterane $\alpha\beta\beta/(\alpha\beta\beta + \alpha\alpha\alpha)$; T20/23: C_{20}/C_{23} tricyclic terpane; Te24/T26: C_{24} tetracyclic terpane/C_{26} tricyclic terpane; Ts/Tm: 18α-22,29,30-trisnorneohopane/17α-22,29,30-trisnorhopane; G/H31: Gammacerane/C_{31} homohopane 22R; H35/34: C_{35}/C_{34} homohopanes; ETR: (TT28 + TT29)/(TT28 + TT29 + Ts); 29Ts/H: 18α-30-norneohopane/17α-30-norhopane.

https://doi.org/10.1021/acsomega.1c03598
ACS Omega 2021, 6, 24106−24117

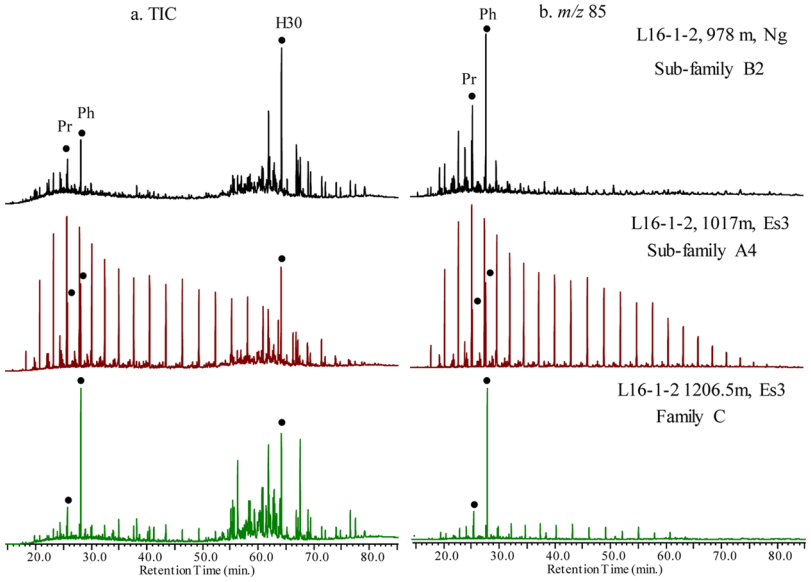

Figure 2. Representative mass chromatograms of the saturated hydrocarbon fraction (a) TICs and (b) m/z 85 mass chromatograms (Pr: pristine; Ph: phytane; H30: C_{30} hopane).

hypersaline reducing environment and is mainly composed of dark-gray mudstone, salt, gypsum, siltstone, and sandstone. The Es3 member was deposited in saline-to-freshwater environments and consists of dark-gray mudstone and black shale with some sandstone. The Es2 member was deposited in a shallow lake and fluvial system and contains principally interbedded grayish-green sandstone and mudstone with thin coal seams. The Es1 member was deposited in another lake transgressive stage and is composed of gray mudstone and siltstone with dolomite. The Dongying Formation was deposited continuously with the Es1 member in the main sag and comprises mainly interbedded grayish-green mudstone and sandstone, while an uplift resulting in a disconformity between the Shahejie and the Dongying formations in the northeastern sag.[8,9] The Neogene Guantao and Minghuazhen formations were deposited in the braided fluvial system and are dominated by grayish-green mudstone, grayish sandy conglomerate, siltstone, and fine sandstone.[15] Since the northeastern sag is a typical marginal sag and its prototype was formed from uplift during the Ek−Es4 stages, no corresponding strata were deposited.[9] The Es4 and Es3 members are the main hydrocarbon source rocks in the main sag, while the Es3 and Es1 members are the main source rock in the northeastern sag. However, the Es1 source rocks, primarily composed of types II1−II2 kerogen, currently are immature to marginally mature and have limited hydrocarbon generation.[8] The reservoirs in the Laizhouwan depression occur in various ages ranging from the Ek to the Nm formations.[5] Shales and mudstone in the Paleogene strata serve as local cap rocks, while mudstones in the Neogene generally serve as regional cap rocks.

3. SAMPLES AND METHODS

The oil-sand bitumen or crude oil samples in this study were collected from nine wells situated at seven blocks in the Laizhouwan depression, which are reservoired in the Minghuazhen, Guantao, Dongying, Shahejie, and Kongdian formations. Wherever possible, multiple samples with different depths, often being sidewall coring sandstones, were collected in the same well, which is helpful in understanding the compositional heterogeneities vertically. Figure 1a displays the well location from which samples were taken. Table 1 shows the basic geological information and geochemical parameters for the studied samples.

The oil-sand samples were crushed into smaller pieces and then extracted using chloroform to get extracted bitumens. The oils or bitumens were deasphaltened by addition of excess light petroleum ether. The maltene fraction was separated into fractions of saturated hydrocarbons, aromatic hydrocarbons, and resins by liquid chromatography on a silica gel/alumina column with different solvents using the same method as described by Zhu et al.[17] The saturated hydrocarbon fraction was eluted by light petroleum ether, the aromatic hydrocarbon fraction was eluted by dichloromethane, and the resin fraction was eluted by a mixture of chloroform and ethanol.

The saturated hydrocarbon fraction was analyzed with a gas chromatograph coupled to a Thermo Fisher Trace-DSQII instrument. A fused silica capillary column (60 m × 0.25 mm) coated with HP-5MS (film thickness 0.25 μm) was used with helium as the carrier gas at a constant flow of 1.0 mL min^{-1}. The injector temperature was 300 °C, with the oven programmed from an initial temperature of 50 °C for 1 min, followed by heating at 15 °C min^{-1} to 100 °C, then at 2 °C min^{-1} to 200 °C, and then at 1 °C min^{-1} to 315 °C with a final holding time for 20 min. The mass spectrometer was operated in the selected ion monitoring mode. Typical MSD conditions were an ionization energy of 70 eV, source temperature of 280 °C, filament current of 100 μA, and electron multiplier voltage of 1.2 kV. Individual compounds were identified on the basis of mass spectrometry and retention index in comparison with the literature. The relative abundance of the compound was estimated using peak areas in the mass chromatogram of characteristic ions. No response factor calibration has been performed.

Pirouette software version 4.5 (Infometrix, Inc.) was employed for chemometric analysis. Hierarchical cluster analysis (HCA) settings: preprocessing: none; distance: Euclidean; linkage method: complete; orientation: sample; transforms: normalize (100). Principal component analysis

https://doi.org/10.1021/acsomega.1c03598
ACS Omega 2021, 6, 24106−24117

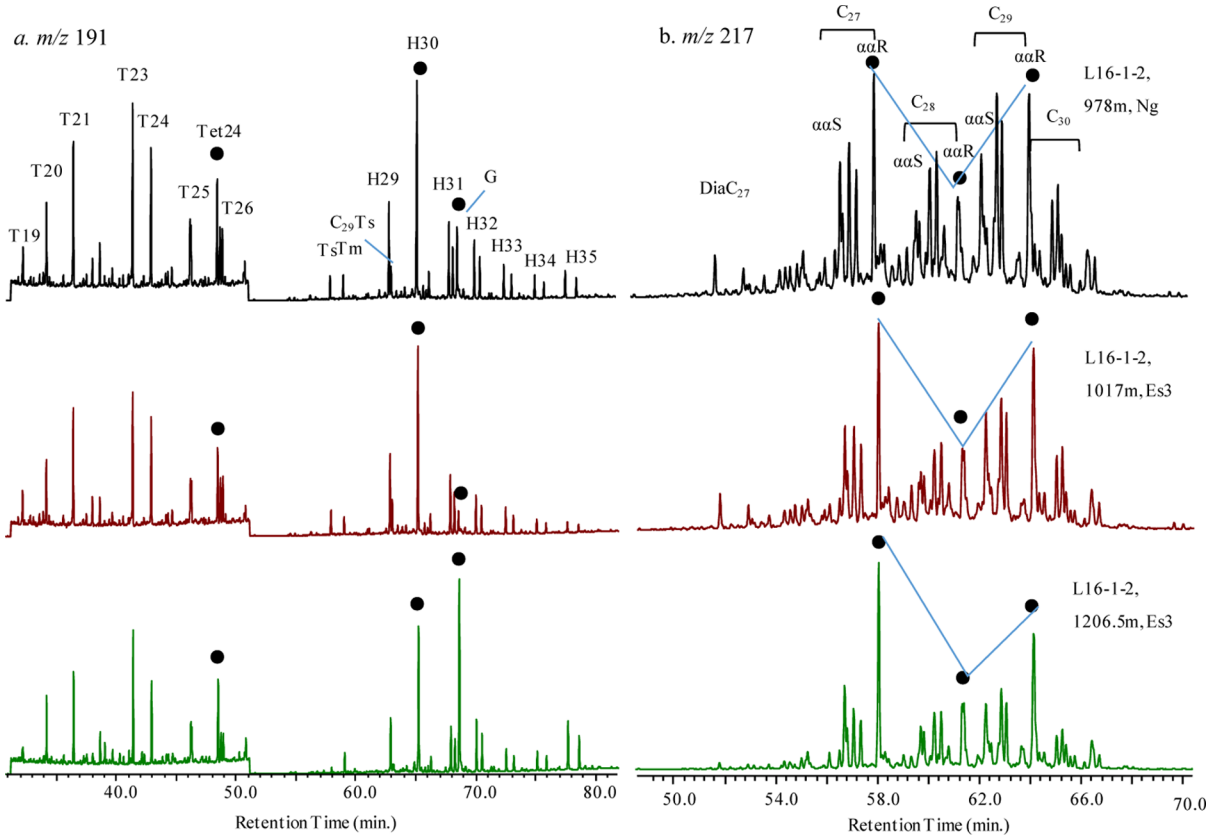

Figure 3. Representative mass chromatograms of m/z 191 (a) and m/z 217 (b) showing the distribution of terpanes and steranes (T19−T26: C_{19}−C_{26} tricyclic terpanes; H29−H35: C_{29}−C_{35} 17α(*H*),21β(*H*)-hopanes; Tet24: C_{24} tetracyclic terpane; Ts: C_{27} 18α(*H*)-22,29,30-trisnorneohopane; Tm: C_{27} 17α(*H*)-22,29,30-trisnorhopane. C_{29}Ts: C_{29} 18α(*H*)-30-norneohopane; G: gammacerane; $\alpha\alpha$R: 5α(*H*),14α(*H*),17α-(*H*) 20R; $\alpha\alpha$S: 5α(*H*),14α(*H*),17α(*H*) 20S).

(PCA) settings: preprocessing: none; maximum factors: 10; optimal factors: 4; validation: none; prob. threshold: 0.95; calib. transfer: not enabled; *Q* threshold: not enabled; transforms: normalize (100).

4. RESULTS AND DISCUSSION

4.1. Overall Molecular Distribution Patterns. Representative total ion chromatograms (TICs) of the saturated hydrocarbon fraction reveal the overall molecular composition changes in the studied samples. Alkanes (*n*-alkanes and isoprenoids) and polycyclic biomarkers (terpanes and steranes) are two main compound classes. Clearly, some samples show great loss of *n*-alkanes and acyclic isoprenoid alkanes leaving the biomarkers (especially hopane series) as the major detectable peaks, while others have plenty of *n*-alkanes and acyclic isoprenoid alkanes with the biomarkers as the minor components (Figure 2).

The compounds detected in the m/z 191 mass chromatograms are tri-, tetra-, and pentacyclic terpanes (Figure 3). The tricyclic terpanes (TTs) can be identified from C_{19} to C_{30} but mainly in the range of C_{19}−C_{26} with a maximum at C_{23}. Only the C_{24} component has been detected in the tetracyclic terpane (TeT) compound class (Figure 3a). The pentacyclic terpanes are dominated by the hopane compound class ranging from C_{27} to C_{35} in majority samples, while a few samples such as oil sand extract from well KL16-1-2 at 1206.5 m have unusually high relative abundance of gammacerane (G), which becomes the highest peak in the m/z 191 mass chromatogram. For the extended hopanes (H31−H35), there are two distinctive distribution patterns: one showing decreasing abundance with increasing carbon number and the other having elevated C_{35} homohopanes (i.e., H35 abundance is higher than H34) (Figure 3a).

In the m/z 217 mass chromatograms, regular steranes, cholestanes (C_{27}), ergostanes (C_{28}), and stigmastanes (C_{29}), as well as their rearranged isomers (diasteranes), were detected in all the samples (Figure 3b). The diasteranes show much lower relative abundance as compared to the regular steranes. The relative abundances of C_{27}, C_{28}, and C_{29} $\alpha\alpha\alpha$ 20R in the samples generally show a "V"-shaped pattern with C_{27} slightly higher than C_{29}. Based on the retention time and mass spectrum, C_{30} 4α-methyl-24-ethylcholestanes have also been detected in variable abundance (Figure 3b).

A series of 25-norhopanes was detected with relatively high abundance in two oil sand extracts from well L10-2-2 at 1399 m and 1474 m and one oil from well L10-5-1 at 1251 m (Figure 4a), indicating heavy biodegradation influence. Interestingly, *n*-alkanes have also been detected in the oil sample from well L10-5-1 (Figure 4b), indicating a mixture of biodegraded oils with fresh charge in the reservoir.

4.2. Effect of Biodegradation on Molecular Compositions. Biodegradation is the main secondary alteration process in shallow reservoirs with temperature <80 °C. Increasing levels of biodegradation generally cause a decline in oil quality and serious problems for oil production, transportation, and refining.[18] Geochemists have made substantial advances in their ability to empirically describe the geochemical sequences of subsurface oil degradation. The

https://doi.org/10.1021/acsomega.1c03598
ACS Omega 2021, 6, 24106−24117

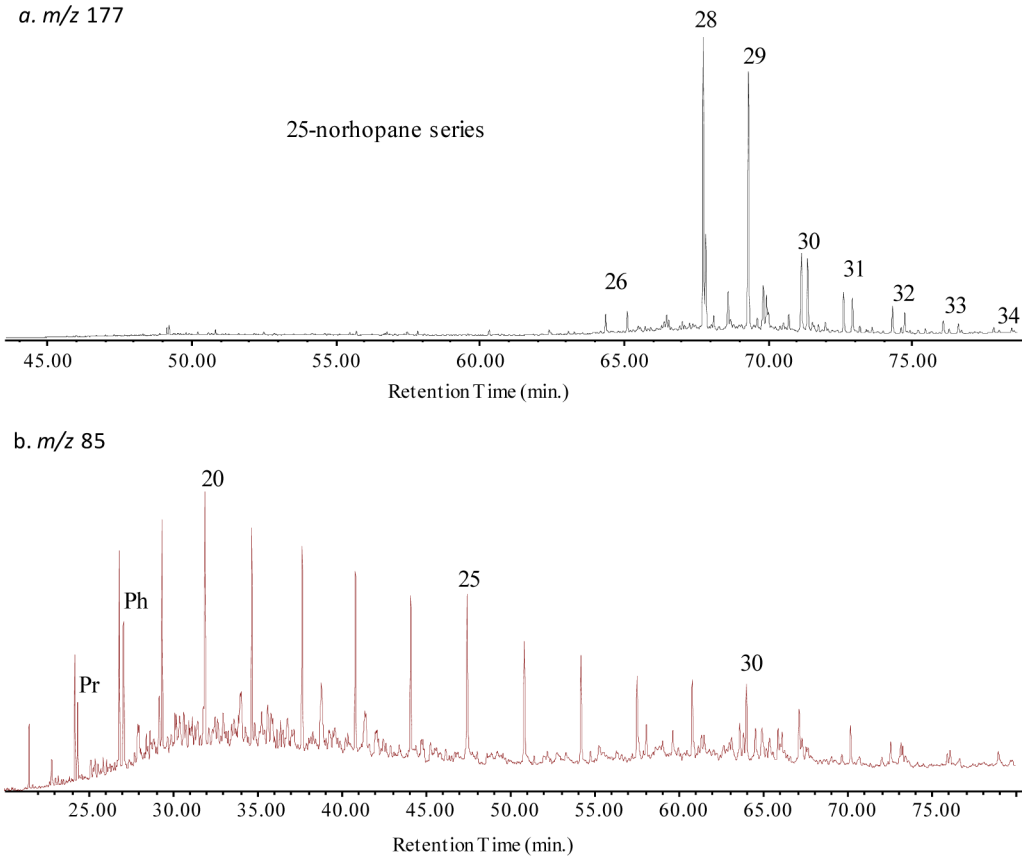

Figure 4. Mass chromatograms of m/z 177 (a) and m/z 85 (b) showing the distribution of the 25-norhopane series and *n*-alkanes and acyclic isoprenoids in the oil sample of L10-5-1 1251m. (Carbon number of the corresponding compound is shown on the peaks.)

effects of biodegradation are most commonly recorded by the variations in the concentration of specific petroleum compounds throughout a reservoir, especially *n*-alkanes and isoprenoid alkanes,[19] alkylaromatic hydrocarbons,[20] nitrogen compounds,[21] and nonhydrocarbons.[22] A "quasi-stepwise" process for hydrocarbon biodegradation, using artificial ranks, has been established based on laboratory experiments and field observations. The 10-point scale proposed by Peters and Moldowan[23] (abbreviated as the PM level) was widely used for biodegradation assessment with PM1 (least altered) to PM10 (most altered). In the 37 samples analyzed in this study, 12 samples show no obvious signs, and 25 samples show variable biodegradation influences. The biodegradation levels in the studied samples estimated on the basis of the PM scale are listed in Table 1. Nonbiodegraded oils are mainly distributed in block L6-4 and the Es3 reservoir in blocks 10-2, 10-4, 10-5, and 16-1. Most oils exhibit light to moderate biodegradation influence. As for light biodegradation influence (PM = 1−3), the pristane (Pr)/*n*-C_{17} and phytane (Ph)/*n*-C_{18} ratios increase with enhanced biodegradation due to preferential loss of the *n*-alkanes, while Pr/Ph values may not be affected. As for moderate biodegradation (PM = 4−5), the *n*-alkanes are largely depleted, while the isoprenoids are severely altered; therefore, the ratios of Pr/Ph, Pr/*n*-C_{17}, and Ph/*n*-C_{18} are invalid for maturity and depositional environment assessment. Once biodegradation approaches a heavy level (PM > 6), parameters derived from hopanes and steranes may lose their validity depending on the severity. Heavy biodegradation has been encountered in three samples from wells L10-2-2 and L10-5-1, where a series of 25-norhopanes has been detected (Figure 4a), but the distributions of hopanes and steranes did not change significantly. A minor proportion of 25-norhopanes has been identified from few other samples with 25-norhopnae/C_{29} hopane ratio <0.2, while majority samples have no 25-norhopanes. However, biodegradation level assignment for the oil sample from well L10-5-1 is complex due to the coexistence of *n*-alkanes and 25-norhopanes. This is a mixed oil with late charge full with *n*-alkanes, but early charged biodegradation residual enriched in 25-norhopanes. The biodegradation level can be assigned in a wide range depending on the reference compound used. Mixing of biodegraded oils with fresh charge may be a common event in the depression; such a case was also noticed in the Liaohe sub-basin, China.[24,25] Nevertheless, the validity of molecular parameters derived from terpanes and steranes has not been significantly deteriorated in the present study samples, while parameters derived from the *n*-alkanes and isoprenoids are affected by biodegradation and have to be excluded from the oil family classification application.

4.3. Molecular Parameters Derived from Terpanes and Steranes. Steranes are derived from steroids (sterols) in eukaryotic organisms such as diatoms, flagellates, zooplanktons, and higher organisms during diagenesis.[26] Generally, sterane distributions reflect the variations in algal input to source rocks and can be used to differentiate crude oils based on genetic relationships. C_{27} steranes are believed to be derived from marine phytoplankton, while abundant C_{29} steranes indicate a contribution from higher plant organic matter and an abundance of C_{28} compounds may indicate the influence of lacustrine algae.[27] However, the abundance of C_{29} steranes are

https://doi.org/10.1021/acsomega.1c03598
ACS Omega 2021, 6, 24106−24117

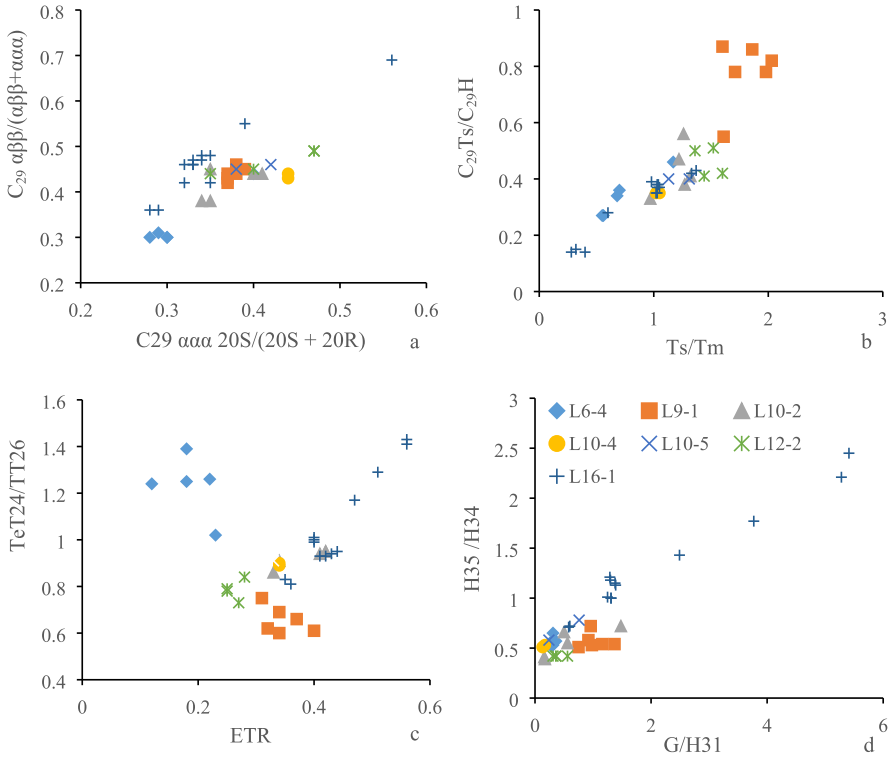

Figure 5. Cross-plots of molecular parameters derived from terpanes and steranes, indicating maturity and depositional environment variation. (a) C_{29} steranes 20S/(20S + 20R) vs $\alpha\beta\beta/(\alpha\beta\beta + \alpha\alpha\alpha)$; (b) Ts/Tm vs $C_{29}Ts/C_{29}H$; (c) ETR vs TeT24/TT26; and (d) G/H31 22R vs H35/H34.

also identified in many algal sources not related to an influence of terrestrial organic matter.[28] The relative abundances of C_{27}, C_{28}, and C_{29} steranes in the studied samples are in the range of 35−57% (averaged 42%), 9−23% (average 16%), and 28−53% (averaged 42%), respectively. The C_{27} steranes are slightly more abundant than C_{29}, but their distributions seem not to be sensitive to oil genetic assessment in the present study and have not been integrated in further investigation.

The apparent isomerization of steranes derives two commonly used maturity parameters. One is based on the isomerization at the C-20 chiral center, involving transformation of the biological 20R configuration into the geological 20S configuration. The other is based on the conversion of biological $\alpha\alpha\alpha$ epimers to geological $\alpha\beta\beta$ epimers.[26] Both 20S/(20S + 20R) and $\alpha\beta\beta/(\alpha\beta\beta + \alpha\alpha\alpha)$ ratios are usually calculated using the C_{29} steranes.[29] The C_{29} $\alpha\beta\beta/(\alpha\beta\beta + \alpha\alpha\alpha)$ ratio varies between 0.30 and 0.55, and the C_{29} $\alpha\alpha\alpha$ 20S/(20S + 20R) ratio ranges from 0.28 to 0.47 in the studied samples, indicating that the oils are marginally mature (Table 1). A general positive correlation can be observed from these two ratios. The samples from blocks L6-4 and L16-1 have lower ratios than others, suggesting low maturity. One oil sand extract from L16-1-1 in the Kongdian formation shows much higher ratios than others with the 20S/(20S + 20R) ratio of 0.56 and $\alpha\beta\beta/(\alpha\beta\beta + \alpha\alpha\alpha)$ ratio of 0.69. As biodegradation is not severe enough to affect sterane distribution in this well, a special origin is inferred. Overall isomerization degrees of steranes indicate that oils in the Laizhouwan depression are thermally less mature to mature (Figure 5a).

The C_{27} pentacyclic triterpane ratio, 18α(*H*)-22,29,30-trisnorneohopane (Ts) versus 17α(*H*)-22,29,30-trisnorhopane (Tm), has been used extensively as an indicator of maturity in samples containing similar source materials. Tm is believed to represent as the biologically produced structure, while Ts is the converted form during thermal maturity processes and exhibits a greater thermal stability than Tm.[29] However, the ratio is also affected by lithology and oxicity of the depositional environment.[30] The Ts/Tm ratio in the studied samples varies from 0.28 to 2.03 (Table 1). Likewise, the C_{29}Ts (18α(*H*)-30-norneohopane) shows the same genetic origin as Ts and the ratio of $C_{29}Ts/C_{29}H$ increases markedly with increasing maturity, but this ratio is also organofacies-related.[23] The $C_{29}Ts/C_{29}$ hopane ratio ranges from 0.14 to 0.87. The Ts/Tm and $C_{29}Ts/C_{29}H$ ratios are almost linearly correlated. The lower ratios mainly occur in block L16-1, while higher ratios are concentrated in block L9-1 (Table 1, Figure 5b). When degrees of sterane isomerization and hopane rearrangement are compared (Figure 5a,b), both maturity and organofacies influences on the relative abundance of Ts and C_{29}Ts can be inferred.

Homohopane isomerization ratios are typically used as maturity indicators for immature to early mature source rocks. Both C_{31} and C_{32} 22S/(22S + 22R) ratios increase sharply from 0.1 at immature samples to reach the equilibrium value of 0.55−0.60 by Ro ∼0.55% just coinciding with the hydrocarbon generation threshold.[26,29] Therefore, the 22S/(22S + 22R) ratio appears to provide no reliable and sensitive indication of maturity for oil as 22S and 22R already reached the equilibrium point in early oil generation window. In this study, most samples have the ratio of C_{31} 22S/(22S + 22R) homohopane ranging between 0.57 and 0.60 at the equilibrium values, indicating that the early oil generation phase has been reached. The purpose to list the C_{31} homohopane 22S/(22S + 22R) ratio in Table 1 is to verify biodegradation influence on hopane distribution and validity of hopane-derived parameters. If severe biodegradation is involved, the 22S/(22S + 22R) ratio will be altered due to the preferential degradation of the 22R

https://doi.org/10.1021/acsomega.1c03598
ACS Omega 2021, 6, 24106−24117

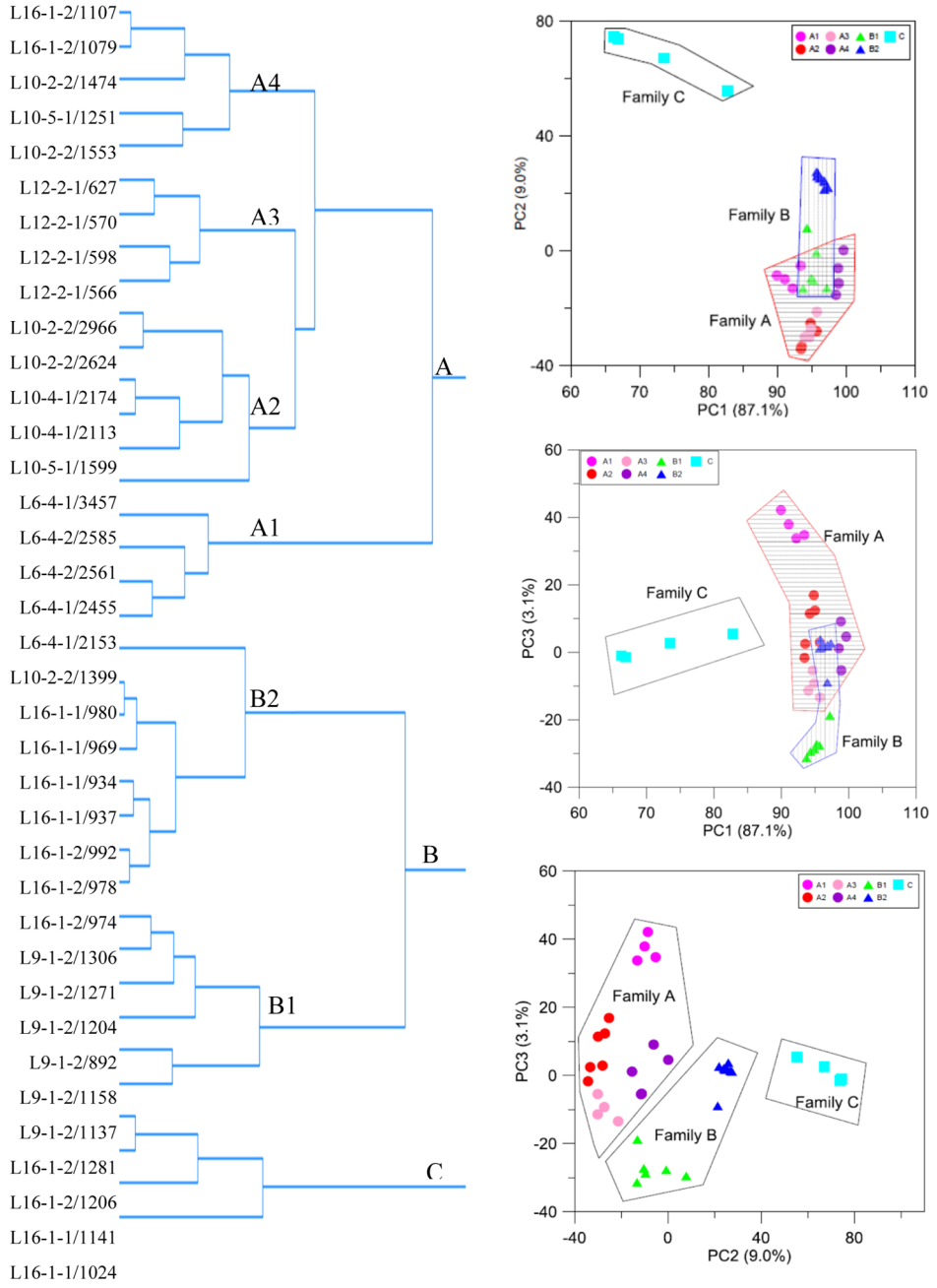

Figure 6. HCA dendrogram (left) and two-dimensional score plots (right) by PCA.

epimer.[31] The C_{31} 22S/(22S + 22R) ratio in this study varies in the narrow range of 0.55−0.63 with an average value of 0.58 except the oil sample from well L10-4-1, whose ratio is 0.67 (Table 1), suggesting that biodegradation does not alter the distribution pattern of pentacyclic terpanes. Therefore, parameters derived from them mainly reflect maturity or depositional environments rather than biodegradation.

The tricyclic terpanes are much less abundant as compared to the pentacyclic terpanes in the studied samples. The TT23/H30 ratio varies in the range of 0.01−0.15 with an average of 0.05 except three heavily biodegraded samples, whose TT23/H30 ratio is in the range of 0.17−0.32. The ratio of TT23/H30 generally increases with maturity, but a significant change is caused by biodegradation. The ratios of various tricyclic terpanes by the carbon number have been acknowledged to give some insights into the source of the organic material. The ratio of C_{20}/C_{23} tricyclic terpane (TT20/TT23) is the most commonly used tricyclic terpane parameter for organic source input assessment. Tricyclic terpanes with the C_{23} component as the dominant peak indicate a marine depositional setting or algae-dominated organic matter input, while the C_{20} component is more enriched in the terrigenous depositional setting.[32] However, this ratio is also sensitive to maturity variation, especially at the high-maturity stage.[33] The ratio of TT20/TT23 varies in the range of 0.28−0.75, reflecting the dominance of algae input in the source rocks. Subtle variation of the TT20/TT23 ratio mainly reflects the change of organic input (Table 1).

The relative abundance of C_{24} tetracyclic terpane (TeT24) is closely related to some depositional environments and/or organic input despite its biological precursor remaining uncertain. High abundance of C_{24} tetracyclic terpane in oils

https://doi.org/10.1021/acsomega.1c03598
ACS Omega 2021, 6, 24106−24117

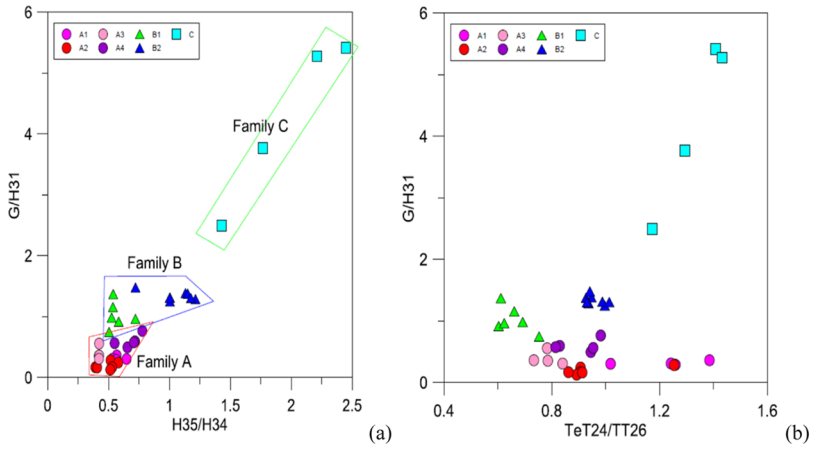

Figure 7. Oil family classification for oils and oil sand bitumens from the Laizhouwan depression. (a) Cross-plot of gammacerane/C_{31} homohopane ratio vs C_{35}/C_{34} homohopane ratio and (b) cross-plot of gammacerane/C_{31} homohopane 22R ratio vs C_{24} tetracyclic terpane/C_{26} tricyclic terpane ratio.

is commonly indicative of terrigenous organic matter input, but it is also enriched in some carbonates and evaporite source-rock settings.[34−36] The ratio of TeT24/TT26 has been widely applied as a molecular parameter to differentiate terrigenous from marine, correlate crude oils, and source rock extracts, predict source rock characteristics, and decipher source rock lithology.[12,32,37] The TeT24/TT26 ratio in the present study varies in the range of 0.61−1.42. Samples with high TeT24/TT26 ratio (>1.0) are mainly distributed in blocks L6-4 and L16-1, while samples with low TeT24/TT26 ratio (<0.8) are largely accumulated in block L9-1 (Table 1).

The extended tricyclic terpane ratio [ETR = (TT28 + TT29) /(TT28 + TT29 + Ts)] was originally proposed by Holba et al.[38] to distinguish Triassic- from Jurassic-sourced oils. Oils with a high ETR value are derived from source rocks deposited in upwelling environments, while those with low ETR values are mainly formed in normal marine environments. Hao et al.[12] suggested that ETR can be used more properly as an indicator of salinity and alkalinity. ETR of ≤0.6 suggests source rock deposition in freshwater-dominated, suboxic, or dysoxic environments with substantial terrigenous organic matter input, while ETR of ≥0.6 suggests source rock deposition in high-salinity and highly reducing environments with minor terrigenous influence. Huang et al.[39] noted that ETR is not an age-related indicator, which can be altered by various other processes such as maturity, biodegradation, and in-reservoir mixing. The ETR in the present studied samples ranges from 0.12 to 0.56, mainly indicating fresh to saline water depositional systems based on the criteria of Hao et al.[12] (Table 1). A cross-plot of TeT24/TT26 ratio versus ETR shows interesting distribution patterns, especially for samples from blocks L6-4 and L16-1, in which the TeT24/TT26 ratio is high, but ETR is situated at low (block L6-4) and high (L16-1) ends, suggesting that different mechanisms govern the variation of the TeT24/TT26 ratio (Figure 5c).

Gammacerane is considered to be a reduction product of tetrahymanol sourced from bacterivorous cliates,[40] which develop at the interface between oxic and anoxic zones in stratified water columns.[41] Although a stratified water column can result from both hypersalinity at depth and temperature gradient, high amounts of gammacerane are usually attributed to evaporite or high-salinity environments,[42] representing strongly reducing characteristics for the source depositional system.[43] Gammacerane abundance was successfully applied in the oil classification in the adjacent Bozhong sub-basin[12] and other depositional basins in China.[17,44,45] The relative abundance of gammacerane showed marked variance in the samples with the gammacerane/C_{31} homohopane 22R (G/H31) ratio in the range of 0.13−5.41. Samples with a high G/H31 ratio are mainly situated at block L16-1 (Table 1).

Homohopanes (H31−H35) are generally believed to originate from bacteriohopanepolyols in the lipid cell membranes of many bacteria.[46] The C_{35} homohopanes are selectively preserved by sulfur incorporation under anoxic conditions, while C_{31}−C_{34} homologues are preferentially preserved under suboxic to oxic conditions due to side-chain cleavage.[47] A commonly used indicator of depositional conditions of source rocks is the homohopane index [HHI = $C_{35}/\Sigma(C_{31} - C_{35})(22S + 22R)$].[48] The ratio of H35/H34 has similar geochemical implication as HHI. Generally, oils and bitumens derived from highly reducing environments of deposition contain high relative abundance of C_{32}−C_{35} homohopanes, while those from freshwater lacustrine environments have low abundance of homohopanes, especially C_{33}−C_{35} homohopanes.[42] The preservation of distinctive carbon numbers of extended hopanes appears to be controlled by the availability of free oxygen during deposition.[48] The values of the C_{35}/C_{34} homohopane (H35/H34) ratio are in the range of 0.39−2.45 (Table 1). The H35/H34 ratios show a linear correlation with the G/H31 ratios, which separates samples in different areas (Figure 5d).

4.4. Oil Family Classification. The classification of the genetic types of crude oils and oil-source correlations is an important part of geochemical research. Petroleum system determination, migration route recognition, and satellite oilfield reconnaissance, and reservoir continuity assessment are part of extensive applications of geochemical correlation studies.[49] Oil genetic classification largely relies on biomarker ratios in the chemometric methods such as PCA and HCA.[50,51] Other genetically related parameters such as bulk composition of oil,[52] carbon isotopic compositions of saturated and aromatic hydrocarbons,[45,53] and Fourier transform infrared spectroscopy of asphaltene subfractions[54] can be also integrated to the chemometric approach. The chemometric method can be used to extract major information from a large number of geochemical parameters, and plenty of information

https://doi.org/10.1021/acsomega.1c03598
ACS Omega 2021, 6, 24106−24117

can be obtained from oil family identification for better understanding their sources, evolutions, and secondary alterations.

In this work, HCA and PCA were used to classify the samples analyzed here using a data set of 37 samples with 9 parameters (Table 1). As shown in Figure 6, three main families (A, B, and C) were classified by HCA and PCA. In composition, family A samples are characterized by a relatively low abundance of gammacerane with the G/H31 ratio in the range of 0.13−0.76, as well as a relatively low abundance of C_{35} homohopane with the ratio of H35/H34 in the range of 0.39−0.78. In contrast, family C samples show relatively high values of G/H31 (2.49−5.41) and H35/H34 (1.43−2.45). Family B samples generally fall in middle values of G/H31 and H35/H34 between family A and C. High G/H31 and H35/H34 ratios in family C oils reflect salinity stratification and are a marker for photic zone anoxia during source rock deposition, which is expected from the Es4 source rocks, whereas low gammacerane and homohopane indexes in family A oils indicate no stratified water or very low salinity in the paleolake during the deposition of the source kitchen, consistent with the features of the Es3 source rocks. These families were well separated in the cross-plot of G/H31 and H35/H34 (Figure 7a). Therefore, family C oils, typically characterized by high gammacerane, should originate from source rocks developed in a hypersaline water depositional system, while family A samples with low gammacerane should be attributed to a freshwater depositional system developed in the depression. Similar two end-member oils were also noticed by Yu et al.[7]

In more detail, family A samples can be further classified into four subfamilies (A1, A2, A3, and A4) by HCA, as shown in Figure 6. As for the four subfamilies, the distinct variation seems to be in the ratio of C_{24}TeT/C_{26}TT. The subfamily A1 oils generally have a high C_{24}TeT/C_{26}TT ratio, subfamily A3 oils display relatively low ratio, and subfamily A2 and A4 oils show intermediate ratio values. Similarly, family B samples can also be further classified into two subfamilies (B1 and B2) by HCA (Figure 6), and the subfamily B1 and B2 samples also show a marked difference in the ratio of C_{24}TeT/C_{26}TT. Besides the family C samples, the subfamilies (A1, A2, A3, A4, B1, and B2) seem to show a good separation with few scatter samples.

A cross-plot of G/H31 versus TeT24/TT26 (Figure 7b) shows that different mechanisms govern the occurrence of TeT24 in the studied oils. High abundance of TeT24 in family C oils is consistent with carbonate lithology in the Es4 source rock system, while high abundance of TeT24 in subfamily A1 oils seems related to terrestrial organic matter input as the G/H31 ratio and ETR are low in family A oils (Figures 5c and 7b). Therefore, the marked variation of TeT24 in the subfamilies, classified by HCA in this study, may be an indicator for differences in source environments and/or organic inputs from the source rock kitchens in the depression.

4.5. Occurrence for the Oil Families and/or Subfamilies. Regular occurrence of oil families or subfamilies is very helpful in petroleum exploration to understand the oil systems in the depositional basins. As mentioned above, the three broad oil families, A, B, and C, were identified for oils in the Laizhouwan depression. Family A oils, with a relatively low abundance of gammacerane and C_{35} homohopanes, were commonly observed in all oilfields widespread in the whole study area. Family C oils, with high amounts of gammacerane and C_{35} homohopanes, locally occurred in the L16-1 block located in the southern part of the study area (Figure 1a). Considering the potential source rocks developed in the depression,[1,3,5,6] family A and C may be extrapolated to end-member oils sourced from distinctive depositional environments. Family A oils were mainly sourced from a freshwater system developed in the Es3 member, which is widely distributed in the whole depression; family C oils were mainly sourced from a hypersaline water system developed in the Es4 member, which is restrictedly distributed in the main sag, while family B oils resulted from the mix of family A and C oils.

With regard to the subfamily oils discussed above, a regular occurrence was observed in the study area. Subfamily A1 oils mainly occurred in the block L6-4 located at the northeast of the study area, subfamily B1 oils were discovered in well L9-1-2 located in the west of the study area, while subfamily A2, A3, and A4 oils were generally distributed in the central region of the study area (Figure 1a). Variations in C_{24} tetracyclic terpane were supposed to be closely related to depositional environments and/or organic matter input in the adjacent Bozhong sub-basin.[12] In combination with the petroleum geology characteristics in the Laizhouwan depression,[9,14] the regular variations of C_{24} tetracyclic terpane from the northeastern sag to the west of the study area may indicate that subfamilies A1, A2, A3, A4, and B1 were mainly attributed from different source sags and/or different source intervals developed with subtle changes in the environment and/or organic input within the freshwater depositional system.

As for the southern region of the depression (main sag), the oils were mainly revealed in block L16-1 where all three oil families can be recognized. A detailed investigation of the oil family and/or subfamily in well L16-1-2 clearly shows an interesting vertical variation. Subfamily B2 oils were trapped in the upper intervals within the Ng Formation, subfamily A4 oils were trapped in the middle intervals within the Es3 reservoirs, whereas family C oils were trapped in the lower intervals within the lower Es3 and Ek reservoirs. The regular occurrence of the oil families and subfamilies (B2, A4, and C) in the block L16-1 clearly indicated that there are at least three oil charges in the area. Moreover, subfamily B2 and family C oils suffered from moderate biodegradation at the degree of about PM 3−5, while subfamily A4 oils with plenty *n*-alkanes show almost no signs of biodegradation (Figure 2, Table 1), indicating that the A4 oils should be the last charge laterally from the northern sag.

5. CONCLUSIONS

Chemometric analysis of nine parameters that are related to thermal maturity, organic matter input, and depositional environment for 37 crude oil and oil sand bitumen samples from the Laizhouwan depression, Bohai Bay basin, reveals three broad oil families, A, B, and C, occurring in the Tertiary depositional system. Family A was derived from the Es3 source rocks deposited under brackish to freshwater environments, while family C originated from the Es4 source rocks deposited in saline to hypersaline water depositional environments. Family B was a composite of two end members distributed mainly in the southwest region. Detailed compositional analyses illustrated that family A and B oils can be further divided into a few subfamilies (A1, A2, A3, A4, B1, and B2) due to subtle organofacies variation and/or different mixing ratios. Vertical compositional heterogeneity in the well L16-1 structure suggests that at least three oil charge events occur in the studied region with the earliest charge from family C and

https://doi.org/10.1021/acsomega.1c03598
ACS Omega 2021, 6, 24106−24117

the latest from subfamily A4. The compositional heterogeneities and genetic affinities of the oils deepen our understanding of petroleum systems in more detail and will facilitate future exploration in the Laizhouwan depression.

AUTHOR INFORMATION

Corresponding Author

Haiping Huang − *School of Geosciences, Yangtze University, Wuhan 430100 Hubei, P. R. China; Department of Geoscience, University of Calgary, Calgary AB T2N 1N4, Canada;* orcid.org/0000-0001-5548-0935; Email: huah@ucalgary.ca

Authors

Zhongjian Tan − *CNOOC China Limited, Tianjin 300459, China*

Jiawei Guo − *School of Geosciences, Yangtze University, Wuhan 430100 Hubei, P. R. China*

Complete contact information is available at: https://pubs.acs.org/10.1021/acsomega.1c03598

Notes

The authors declare no competing financial interest.

ACKNOWLEDGMENTS

This study was financially supported by the National Natural Science Foundation of China (nos. 41730424 and 41873049). We appreciate the collaboration of Yun Hu, Min Mao, Qingbin Wang, and Hongru Li at the Tianjin Branch of China National Offshore Oil Company Ltd. Prof. Frank Quina and two anonymous reviewers are acknowledged for their constructive comments, which improve the quality of this paper substantially.

REFERENCES

(1) Yang, B.; Niu, C.; Sun, H.; Wang, L.; Wang, G. The significance of discovering Kenli 10-1 oilfield in 10^8 ton-reserves grade in Laizhouwan sag. *China Offshore Oil Gas* **2011**, *23*, 10−15.

(2) Yang, B.; Hu, Z.; Li, G.; Yang, H. Tectonic characteristics and hydrocarbon accumulation rules in south slope of Laizhouwan sag in Bohai sea. *China Offshore Oil Gas* **2016**, *28*, 22−29.

(3) Niu, C. Tectonic evolution and hydrocarbon accumulation of Laizhouwan depression in southern Bohai Sea. *Oil Gas Geol.* **2012**, *33*, 424−431.

(4) Niu, C.; Chen, L.; Yang, B.; Zhang, B.; Wang, S.; Guo, X. Structure characteristics of KL16−A and its control to reservoir in the southern slope of Laizhouwan Sag. *Oil Geophys. Prospect.* **2018**, *53*, 1067−1074.

(5) Wang, G.-z.; Niu, C.; Wang, L.; Ye, X. Enlightenments of exploration breakthrough in Laizhouwan Depression. *J. Oil, Gas Technol.* **2012**, *34*, 39−43.

(6) Tang, G.; Wang, F.; Wang, Q.; Wan, L.; Yan, G. Genesis and accumulation models of sulfur-rich heavy oil in Laizhou Bay Sag, Bohai Sea. *Oil Gas Geol.* **2019**, *40*, 284−293.

(7) Yu, Q.; Xu, G.; Liang, H.; Xu, F.; Liang, J.; Wang, D. A research into the crude oil geochemistry and oil-source correlation by means of gas chromatography and gas chromatography−mass spectrometry: a case study of the Laizhou Bay Sag, Bohai Bay Basin, China. *Arabian J. Geosci.* **2019**, *12*, 634.

(8) Zhao, Z.; Hou, D.; Cheng, X.; Xu, H.; Ma, C.; Zhou, X.; Xu, C. Geochemical and palynological characteristics of the Paleogene source rocks in the Northeastern Laizhouwan Sag, Bohai Bay Basin, China: Hydrocarbon potential, depositional environment, and factors controlling organic matter enrichment. *Mar. Pet. Geol.* **2021**, *124*, 104792.

(9) Peng, W.; Xin, R.; Sun, H.; Wu, K.; Shi, H.; Wang, D. Formation and evolution of Laizhou Bay sag in Bohai Bay. *Acta Petrol. Sin.* **2009**, *30*, 654−660.

(10) Huang, H.; Pearson, M. J. Source rock palaeoenvironments and controls on the distribution of dibenzothiophenes in lacustrine crude oils, Bohai Bay Basin, eastern China. *Org. Geochem.* **1999**, *30*, 1455−1470.

(11) Hao, F.; Zou, H.; Gong, Z.; Deng, Y. Petroleum migration and accumulation in the Bozhong sub-basin, Bohai Bay basin, China: Significance of preferential petroleum migration pathways (PPMP) for the formation of large oilfields in lacustrine fault basins. *Mar. Pet. Geol.* **2007**, *24*, 1−13.

(12) Hao, F.; Zhou, X.; Zhu, Y.; Zou, H.; Bao, X.; Kong, Q. Mechanisms of petroleum accumulation in the Bozhong sub-basin, Bohai Bay Basin, China. Part 1: Origin and occurrence of crude oils. *Mar. Pet. Geol.* **2009**, *26*, 1528−1542.

(13) Yu, Z.; Wu, S.; Zou, D.; Feng, D.; Zhao, H. Seismic profiles across the middle Tan-Lu fault zone in Laizhou Bay, Bohai Sea, eastern China. *J. Asian Earth Sci.* **2008**, *33*, 383−394.

(14) Xin, Y.; Ren, J.; Li, J. Control of tectonic-paleogeomorphology on deposition: A case from the Shahejie Formation Sha 3 member, Laizhouwan Sag, southern Bohai Sea. *Pet. Explor. Dev.* **2013**, *40*, 325−332.

(15) Yu, Y.; Zhou, X.; Tang, L.; Peng, W.; Lu, D.; Li, W. Salt structures in the Laizhouwan depression, offshore Bohai Bay basin, eastern China: New insights from 3D seismic data. *Mar. Pet. Geol.* **2009**, *26*, 1600−1607.

(16) Huang, L.; Wang, Y.; Wu, Q.; Wang, Q. Cenozoic tectonic evolution of the Laizhouwan Sag in Bohai Bay Basin. *Acta Geol. Sin.* **2012**, *86*, 867−876.

(17) Yangming, Z.; Huanxin, W.; Aiguo, S.; Digang, L.; Dehua, P. Geochemical characteristics of Tertiary saline lacustrine oils in the Western Qaidam Basin, northwest China. *Appl. Geochem.* **2005**, *20*, 1875−1889.

(18) Head, I. M.; Jones, D. M.; Larter, S. R. Biological activity in the deep subsurface and the origin of heavy oil. *Nature* **2003**, *426*, 344−352.

(19) Wenger, L. M.; Davis, C. L.; Isaksen, G. H. Multiple controls on petroleum biodegradation and impact on oil quality. *SPE Reservoir Eval. Eng.* **2002**, *5*, 375−383.

(20) Huang, H.; Bowler, B. F. J.; Oldenburg, T. B. P.; Larter, S. R. The effect of biodegradation on polycyclic aromatic hydrocarbons in reservoired oils from the Liaohe basin, NE China. *Org. Geochem.* **2004**, *35*, 1619−1634.

(21) Huang, H.; Bowler, B. F. J.; Zhang, Z.; Oldenburg, T. B. P.; Larter, S. R. Influence of biodegradation on carbazole and benzocarbazole distributions in oil columns from the Liaohe basin, NE China. *Org. Geochem.* **2003**, *34*, 951−969.

(22) Liao, Y.; Geng, A.; Huang, H. The influence of biodegradation on resins and asphaltenes in the Liaohe Basin. *Org. Geochem.* **2009**, *40*, 312−320.

(23) Peters, K.; Moldowan, J. M. *The Biomarker Guide: Interpreting Molecular Fossils in Petroleum and Ancient Sediments*; Prentice Hall: Englewood Cliffs, NJ, 1993.

(24) Koopmans, M. P.; Larter, S. R.; Zhang, C.; Mei, B.; Wu, T.; Chen, Y. Biodegradation and mixing of crude oils in Eocene Es3 reservoirs of the Liaohe basin, northeastern China. *AAPG Bull.* **2002**, *86*, 1833−1843.

(25) Huang, H.; Larter, S. R.; Bowler, B. F. J.; Oldenburg, T. B. P. A dynamic biodegradation model suggested by petroleum compositional gradients within reservoir columns from the Liaohe basin, NE China. *Org. Geochem.* **2004**, *35*, 299−316.

(26) Mackenzie, A. S.; Mackenzie, A. S. Application of biological markers in petroleum geochemistry. In *Advances in Petroleum Geochemistry I*; Brooks, J., Welte, D., Eds.; Academic Press: London, 1984; pp 115−214.

(27) Huang, W.-Y.; Meinschein, W. G. Sterols as ecological indicators. *Geochim. Cosmochim. Acta* **1979**, *43*, 739−745.

(28) Volkman, J. K.; Barrett, S. M.; Blackburn, S. I.; Mansour, M. P.; Sikes, E. L.; Gelin, F. Microalgal biomarkers: A review of recent research developments. *Org. Geochem.* **1998**, *29*, 1163−1179.
(29) Seifert, W. K.; Moldowan, J. M. Use of biological markers in petroleum exploration. In *Biological Markers in the Sedimentary Record 24, Methods in Geochemistry and Geophysics*; Johns, R. B., Ed.; Elsevier, 1986: pp 261−290.
(30) Rullkötter, J.; Marzi, R. Natural and artificial maturation of biological markers in a Toarcian shale from northern Germany. *Org. Geochem.* **1988**, *13*, 639−645.
(31) Peters, K. E.; Moldowan, J. M.; McCaffrey, M. A.; Fago, F. J. Selective biodegradation of extended hopanes to 25-norhopanes in petroleum reservoirs. Insights from molecular mechanics. *Org. Geochem.* **1996**, *24*, 765−783.
(32) Neto, F. R. A.; Cardoso, J. N.; Rodrigues, R.; Trindade, L. A. F. Evolution of tricyclic alkanes in the Espirito Santo Basin, Brazil. *Geochim. Cosmochim. Acta* **1986**, *50*, 2069−2072.
(33) Huang, H.; Zhang, S.; Su, J. Geochemistry of tri-and tetracyclic terpanes in the palaeozoic oils from the Tarim Basin, Northwest China. *Energy Fuels* **2015**, *29*, 7014−7025.
(34) Palacas, J. G.; Anders, D. E.; King, J. D. Florida Basin−a prime example of carbonate source rocks of petroleum. *Geochemistry and Source Rock Potential of Carbonate Rocks*; AAPG Studies in Geology, 1984; Vol. *18*, pp 71−96.
(35) Connan, J.; Bouroullec, J.; Dessort, D.; Albrecht, P.; Leythaeuser, D.; Ruellkotter, J. The microbial input in carbonate-anhydrite facies of a sabkha palaeoenvironment from Guatemala; a molecular approach. *Org. Geochem.* **1986**, *10*, 29−50.
(36) Clark, J. P.; Philp, R. P. Geochemical characterization of evaporite and carbonate depositional environments and correlation of associated crude oils in the Black Creek basin, Alberta. *Bull. Can. Pet. Geol.* **1989**, *37*, 401−416.
(37) Philp, R. P.; Gilbert, T. D. Biomarker distributions in Australian oils predominantly derived from terrigenous source material. *Org. Geochem.* **1986**, *10*, 73−84.
(38) Holba, A. G.; Ellis, L.; Dzou, I. L.; Hallam, A.; Masterson, W. D.; Francu, J.; Fincannon, A. L. Extended tricyclic terpanes as age discriminators between Triassic, Early Jurassic and Middle-Late Jurassic oils. *20th International Meeting on Organic Geochemistry, Abstracts*, 2001; Vol. *1*, p 464.
(39) Huang, H.; Zhang, S.; Gu, Y.; Su, J. Impacts of source input and secondary alteration on the extended tricyclic terpane ratio: A case study from Palaeozoic sourced oils and condensates in the Tarim Basin, NW China. *Org. Geochem.* **2017**, *112*, 158−169.
(40) Haven, H. L. T.; Rohmer, M.; Rullkötter, J.; Bisseret, P. Tetrahymanol, the most likely precursor of gammacerane, occurs ubiquitously in marine sediments. *Geochim. Cosmochim. Acta* **1989**, *53*, 3073−3079.
(41) Sinninghe Damsté, J. S.; Kenig, F.; Koopmans, M. P.; Köster, J.; Schouten, S.; Hayes, J. M.; de Leeuw, J. W. Evidence for gammacerane as an indicator of water column stratification. *Geochim. Cosmochim. Acta* **1995**, *59*, 1895−1900.
(42) Jiamo, J.; Guoying, S.; Jiayou, X.; Eglinton, G.; Gowar, A. P.; Rongfen, J.; Shanfa, F.; Pingan, P. Application of biological markers in the assessment of paleoenvironments of Chinese non-marine sediments. *Org. Geochem.* **1990**, *16*, 769−779.
(43) Moldowan, J. M.; Seifert, W. K.; Gallegos, E. J. Relationship between petroleum composition and depositional environment of petroleum source rocks. *AAPG Bull.* **1985**, *69*, 1255−1268.
(44) Zhang, C.; Zhang, Y.; Zhang, M.; Chen, Z.; Peng, D.; Sun, W.; Cai, C. Compositional variabilities among crude oils from the southwestern part of the Qaidam Basin, NW China. *J. Pet. Sci. Eng.* **2008**, *62*, 87−92.
(45) Zhan, Z.-W.; Lin, X.-H.; Zou, Y.-R.; Li, Z.; Wang, D.; Liu, C.; Peng, P. a. Chemometric differentiation of crude oil families in the southern Dongying Depression, Bohai Bay Basin, China. *Org. Geochem.* **2019**, *127*, 37−49.
(46) Farrimond, P.; Talbot, H. M.; Watson, D. F.; Schulz, L. K.; Wilhelms, A. Methylhopanoids, molecular indicators of ancient bacteria and a petroleum correlation tool. *Geochim. Cosmochim. Acta* **2004**, *68*, 3873−3882.
(47) Köster, J.; Van Kaam-Peters, H. M. E.; Koopmans, M. P.; de Leeuw, J. W.; Sinninghe Damsté, J. S. Sulfurization of homohopanoids, Effects on carbon number distribution, speciation, and 22S 22R epimer ratios. *Geochim. Cosmochim. Acta* **1997**, *61*, 2431−2452.
(48) Peters, K. E.; Moldowan, J. M. Effects of source, thermal maturity and biodegradation on the distribution and isomerization of homohopanes in petroleum. *Org. Geochem.* **1991**, *17*, 47−61.
(49) Hunt, J. H. *Petroleum Geology and Geochemistry*, 2nd ed.; W. H. Freeman and Co.: New York, 1996.
(50) Peters, K. E.; Coutrot, D.; Nouvelle, X.; Ramos, L. S.; Rohrback, B. G.; Magoon, L. B.; Zumberge, J. E. Chemometric differentiation of crude oil families in the San Joaquin Basin, California. *AAPG Bull.* **2013**, *97*, 103−143.
(51) Peters, K. E.; Wright, T. L.; Ramos, L. S.; Zumberge, J. E.; Magoon, L. B. Chemometric recognition of genetically distinct oil families in the Los Angeles basin, California. *AAPG Bull.* **2016**, *100*, 115−135.
(52) Rangel, A.; Osorno, J. F.; Ramirez, J. C.; De Bedout, J.; González, J. L.; Pabón, J. M. Geochemical assessment of the Colombian oils based on bulk petroleum properties and biomarker parameters. *Mar. Pet. Geol.* **2017**, *86*, 1291−1309.
(53) Lin, X.-H.; Zhan, Z.-W.; Zou, Y.-R.; Sun, J.-N.; Peng, P. a. Geochemically Distinct Oil Families in the Gudong Oilfield, Zhanhua Depression, Bohai Bay Basin, China. *ACS Omega* **2020**, *5*, 26738−26747.
(54) Asemani, M.; Rabbani, A. R. A novel and efficient chemometric approach to identifying oil families by saturate biomarker data and FTIR spectroscopy of asphaltene subfractions. *Mar. Pet. Geol.* **2021**, *124*, 104838.

https://doi.org/10.1021/acsomega.1c03598
ACS Omega 2021, 6, 24106−24117